Identification of a highly neurotoxic α-synuclein species inducing mitochondrial damage and mitophagy in Parkinson's disease

Diego Grassi[a,b], Shannon Howard[c], Minghai Zhou[a,b], Natalia Diaz-Perez[d], Nicolai T. Urban[e], Debbie Guerrero-Given[f], Naomi Kamasawa[f], Laura A. Volpicelli-Daley[g], Philip LoGrasso[c], and Corinne Ida Lasmézas[a,b,1]

[a]Department of Immunology and Microbiology, Scripps Florida, The Scripps Research Institute, Jupiter, FL 33458; [b]Department of Neuroscience, Scripps Florida, The Scripps Research Institute, Jupiter, FL 33458; [c]Department of Molecular Medicine Scripps Florida, The Scripps Research Institute, Jupiter, FL 33458; [d]Private address, Palm Beach Gardens, FL 33418; [e]Light Microscopy Facility, Max Planck Florida Institute for Neuroscience, Jupiter, FL 33458; [f]Electron Microscopy Facility, Max Planck Florida Institute for Neuroscience, Jupiter, FL 33458; and [g]Center for Neurodegeneration and Experimental Therapeutics, University of Alabama at Birmingham, Birmingham, AL 35294

Edited by Edward A. Hoover, Colorado State University, Fort Collins, CO, and approved January 24, 2018 (received for review August 11, 2017)

Exposure of cultured primary neurons to preformed α-synuclein fibrils (PFFs) leads to the recruitment of endogenous α-synuclein and its templated conversion into fibrillar phosphorylated α-synuclein (pα-synF) aggregates resembling those involved in Parkinson's disease (PD) pathogenesis. Pα-synF was described previously as inclusions morphologically similar to Lewy bodies and Lewy neurites in PD patients. We discovered the existence of a conformationally distinct, nonfibrillar, phosphorylated α-syn species that we named "pα-syn*." We uniquely describe the existence of pα-syn* in PFF-seeded primary neurons, mice brains, and PD patients' brains. Through immunofluorescence and pharmacological manipulation we showed that pα-syn* results from incomplete autophagic degradation of pα-synF. Pα-synF was decorated with autophagic markers, but pα-syn* was not. Western blots revealed that pα-syn* was N- and C-terminally trimmed, resulting in a 12.5-kDa fragment and a SDS-resistant dimer. After lysosomal release, pα-syn* aggregates associated with mitochondria, inducing mitochondrial membrane depolarization, cytochrome C release, and mitochondrial fragmentation visualized by confocal and stimulated emission depletion nanoscopy. Pα-syn* recruited phosphorylated acetyl-CoA carboxylase 1 (ACC1) with which it remarkably colocalized. ACC1 phosphorylation indicates low ATP levels, AMPK activation, and oxidative stress and induces mitochondrial fragmentation via reduced lipoylation. Pα-syn* also colocalized with BiP, a master regulator of the unfolded protein response and a resident protein of mitochondria-associated endoplasmic reticulum membranes that are sites of mitochondrial fission and mitophagy. Pα-syn* aggregates were found in Parkin-positive mitophagic vacuoles and imaged by electron microscopy. Collectively, we showed that pα-syn* induces mitochondrial toxicity and fission, energetic stress, and mitophagy, implicating pα-syn* as a key neurotoxic α-syn species and a therapeutic target.

Parkinson's disease | mitochondria | toxicity | alpha-synuclein | autophagy

Parkinson's disease (PD) is an age-related protein-misfolding neurodegenerative disease (PMND) affecting over 1 million people in the United States. It is the second most common neurodegenerative disorder after Alzheimer's disease (AD). Approximately 1–2% of the population over the age of 60 y and 4–5% over the age of 85 y suffer from PD (1). PD is characterized by resting tremor, bradykinesia, rigidity, gait disturbance, postural instability and cognitive symptoms. Motor impairment is due to the degeneration of dopaminergic neurons of the substantia nigra pars compacta (SNpc) and subsequent loss of dopamine innervation in the striatum (2). Affected neurons accumulate intracytoplasmic inclusions known as "Lewy bodies" (LBs). There is currently no disease-modifying treatment for PD (3). Approximately 85–90% of PD cases are considered idiopathic. At least five genes, *SNCA*, *GBA*, *PARK2*/*Parkin*, *PINK1*, *DJ-1*, and *LRRK2*, are linked to heritable PD (4, 5). There is compelling evidence for a fundamental role of α-synuclein (α-syn), encoded by the *SNCA* gene, in PD (6–9). α-Syn is the major component of LBs (10). The intracellular accumulation of α-syn is also the hallmark of several disorders referred to as "synucleinopathies," such as dementia with Lewy bodies, the Lewy body variant of AD, or multiple-system atrophy (10–13). Contrasting with the overwhelming evidence for a central role of α-syn in the pathogenesis of PD and other α-synucleinopathies is the limited knowledge about how the abnormal accumulation of this protein leads to neuronal demise. This is the focus of the present study.

To study α-syn and neurotoxicity, we took advantage of the fact that misfolded, aggregated α-syn propagates in neuronal cultures and in mouse and human brains in a prion-like fashion, triggering dysfunction and death of dopaminergic neurons (14–18). Notably, fibrils of recombinant α-syn, called "preformed fibrils" (PFFs), seed the misfolding and aggregation of endogenous α-syn in cell lines and primary neurons, leading to the formation of large Triton-insoluble α-syn fibrils (14, 19, 20). These fibrils are composed of α-syn phosphorylated at S129 (pα-syn), mimicking the formation of LBs in PD patients' brains where >90% of α-syn is phosphorylated at S129 (21). PFF-seeded neurons undergo autophagic failure (22), defective vesicular transport (23), synaptic dysfunction, and neuronal death (20). The PFF seeding model therefore reproduces

Significance

Parkinson's disease (PD) is a neurodegenerative disease linked to the misfolding and aggregation of a protein called "α-synuclein." α-Synuclein aggregates found in the brains of PD patients are called "Lewy bodies" and "Lewy neurites." We discovered the existence of a type of α-synuclein aggregate, smaller than previously described and conformationally distinct, that we called "pα-syn*." Pα-syn* was present in neuronal cultures and mice brains injected with recombinant α-synuclein fibrils as well as in the brains of PD patients. We showed that pα-syn* is made of trimmed α-synuclein resulting from a failed cellular attempt to degrade fibrillar α-synuclein aggregates. We found that pα-syn* is a major neurotoxic species inducing mitochondrial damage, fission, and mitophagy, therefore constituting a central player in PD pathogenesis.

Author contributions: D.G. and C.I.L. designed research; D.G., S.H., M.Z., N.T.U., D.G.-G., and N.K. performed research; L.A.V.-D. contributed new reagents/analytic tools; D.G., M.Z., N.D.-P., N.T.U., N.K., P.L., and C.I.L. analyzed data; and D.G. and C.I.L. wrote the paper.

The authors declare no conflict of interest.

This article is a PNAS Direct Submission.

[1]To whom correspondence should be addressed. Email: lasmezas@scripps.edu.

This article contains supporting information online at www.pnas.org/lookup/suppl/doi:10.1073/pnas.1713849115/-/DCSupplemental.

Published online February 27, 2018.

key features of PD pathogenesis and was used to gain better understanding of the link between α-syn and cellular dysfunction.

Herein, we identified a conformationally distinct pα-syn species that we named "pα-syn*" due to its high biological reactivity. Pα-syn* resulted from incomplete autophagic degradation of fibrillar pα-syn. It associated with mitochondria where it induced membrane depolarization, cytochrome C release, and recruitment of phosphorylated (inactive) acetyl-CoA carboxylase 1 (pACC1), causing structural damage to mitochondrial membranes via reduced lipoylation, lower energy supply, and oxidative stress. Pα-syn* was found in the vicinity of mitochondria-associated endoplasmic reticulum (ER) membranes (MAMs) known to juxtapose to the sites of mitochondrial fission and mitophagy. Finally, pα-syn* was found associated with mitochondrial debris in mitophagic lysosomes. Overall, these results indicate that pα-syn* is highly mitotoxic and a key player in Parkinson's disease pathogenesis.

Results

Seeding of Primary Neurons with α-Syn PFFs Leads to Intracellular Accumulation of Two Conformers of Pα-Syn with Different Morphologies and Cellular Localization: Pα-Syn* and Pα-SynF. Using two different antibodies specific to phosphorylated S129 α-syn, we observed the existence of two distinct types of pα-syn aggregates progressively accumulating over 14 d (Fig. 1). Neuronal demise prevented us from keeping the cultures past 2 wk postseeding. The first to appear and most abundant aggregates were visible as dot-like structures 2–3 d postinduction and rapidly formed elongated, bundled aggregates. This form of pα-syn is known to be fibrillar (20, 23) and was named "pα-synF." As early as day 4, pα-synF presented as long fibers similar to Lewy neurites (LNs) described in PD patients and, starting from day 6, as densely packed cage-like structures around the nucleus, always with a polarity, reminiscent of LBs (Fig. 1, days 11 and 14). In addition, a less abundant, mostly punctate pα-syn entity was also observed, progressively accumulating in areas densely packed with pα-synF in the perinuclear region; this distinctive form of pα-syn was called pα-syn* for "pα-syn STAR" (α-synuclein **t**runcated **a**damant and **r**eactive). Cells exposed to α-syn monomers instead of PFFs did not accumulate pα-syn aggregates (Fig. S1). Pα-syn* was found to accumulate exclusively in neuronal cells (Fig. S2). Cultures were made of ∼70% neuronal cells, with the great majority of nonneuronal cells being astrocytes.

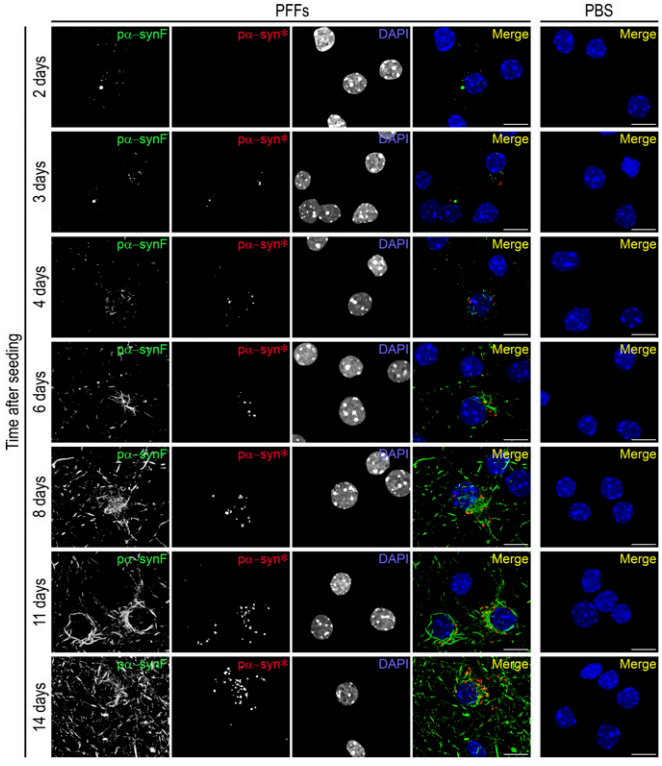

Fig. 1. Time course of the appearance of pα-syn* in PFF-treated neurons. Primary hippocampal mouse neurons were exposed to PFFs at day in vitro (DIV)7 and were examined by immunocytochemistry (ICC) at various time points from days 2–14. Cells similarly treated with PBS alone constitute the control. Pictures show labeling with the pα-syn antibodies recognizing pα-synF or pα-syn*, respectively, and DAPI staining showing the nuclei, color-coded as green, red, and blue, respectively, in the merged image. Neurons from the PBS control were labeled similarly; the merged image is shown. No pα-syn was observed in control cells in our experimental conditions. (Scale bars, 10 μm.)

The strictly selective and mutually exclusive immunoreactivity of pα-syn* and pα-synF toward two different antibodies both recognizing an epitope comprising phosphorylated S129 of pα-syn (polyclonal and monoclonal, respectively, as described in *Materials and Methods*) indicated that these aggregates represent different conformers of pα-syn and that the pα-syn* antibody recognizes a conformational epitope. At this point, we speculated that pα-synF and pα-syn* would share neither the same cellular interactome nor biological effects.

Pα-Syn* Is Also Found in Vivo in PFF-Injected Mice and PD Patients. To establish the relevance of this finding in vivo, we examined the brains of mice stereotaxically injected with PFFs and killed after 30 d. Both pα-synF and pα-syn* inclusions were observed, with morphology and cellular localization remarkably similar to those in the neuronal cultures. Despite the injection being made in the striatum, pα-synF and pα-syn* inclusions were present in both the cortex and the substantia nigra, showing the appearance of pathogenic pα-syn in brain regions that project to the striatum. They were more abundant in the cortex than in the substantia nigra (Fig. 2 and Fig. S3). Importantly, pα-syn* conformers were also observed in brain sections of PD patients, showing the relevance of this pα-syn species to human PD pathogenesis. Similar to our observations in neuronal cultures, pα-syn* aggregates were generally observed in the vicinity of LBs in PD patients' brains (Fig. 2). However, we could not establish a quantitative relationship between the LB burden and the detection of pα-syn*. Patients' characteristics are presented in Table S1.

Pα-Syn* Is a Truncated Pα-Syn Resulting from Incomplete Degradation of Pα-SynF Fibrils. Our next series of experiments led to the discovery that pα-syn* originates from a conformational change within the pα-synF fibrils. This conversion appeared to take place according to three scenarios, depending on the density and thickness of the original pα-synF fibril. It is important to note that these fibrils have been shown earlier to adopt a double-stranded structure (20). The first scenario may be described as the shedding of pα-syn* from low-density, thin pα-synF fibrils (Fig. 3 *A–D*). In this case, pα-syn* appeared to be shed from the fibrils, along with a progressive disintegration of the pα-synF core of the fibrils. Patches of pα-syn* intermingled with patches of pα-synF; ultimately the fibrillar core completely disappeared, and only newly generated pα-syn* aggregates remained (Fig. 3*D*). The second scenario was observed with dense pα-synF fibrils more clearly intertwined in a helical fashion. One strand of the helix unwound and was "digested," giving rise to pα-syn* aggregates decorating the remaining strand (Fig. 3 *E–G*). In a third scenario, dense fibers of pα-synF appeared to undergo conversion into pα-syn* from one end of the fiber, with the conversion progressing toward the other end (Fig. 3*H*). In this case one end of the fibril exhibited pα-synF immunoreactivity, the other end pα-syn* immunoreactivity, and a degradation front was clearly observed (*Inset H2*).

Western blot analysis revealed that pα-syn* is a truncated species of pα-syn migrating at 12.5 kDa (Fig. 3*I*, *Right*, red arrows). Pα-syn* was detected specifically in PFF-treated neurons in both

NEUROSCIENCE

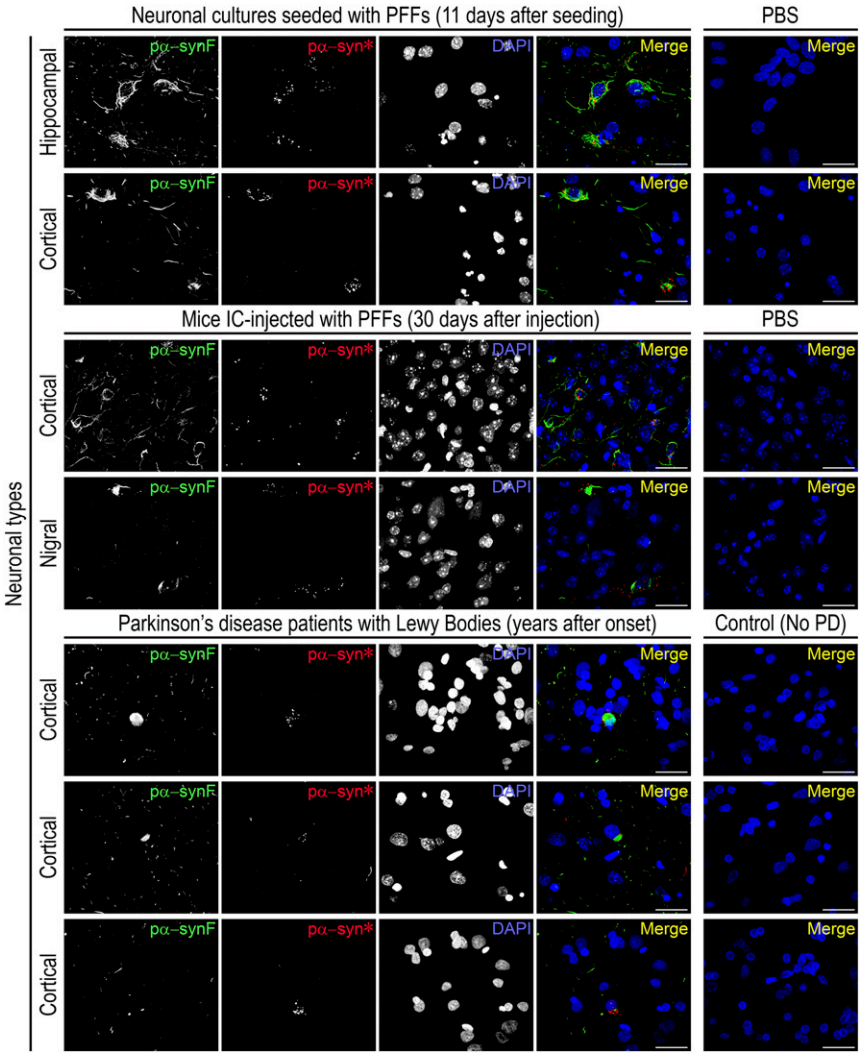

Fig. 2. Detection of both pα-synF and pα-syn* in the brains of PFF-injected mice and PD patients. (*Top*) Mouse hippocampal or cortical primary neurons seeded with PFFs develop pα-synF and pα-syn* inclusions. (*Middle*) Mice stereotaxically injected with PFFs in the striatum develop both pα-synF and pα-syn* inclusions in the cortex and substantia nigra, with morphologies and subcellular localization identical to the cell cultures. (*Bottom*) Both pα-synF and pα-syn* inclusions were observed in the cortex of three LB-harboring patients with PD: case ID10-89 (*Top Row*); case ID12-69 (*Middle Row*); and case ID11-51 (*Bottom Row*) (Table S1). Pα-syn* was also observed in all but one of the high-LB cases and in two of the low-LB cases that we looked at. Note the pα-syn* puncta surrounding the LBs. The LBs are detected using the pα-synF–specific antibody. Labeling for pα-synF, pα-syn*, and DAPI was color-coded as green, red and blue, respectively, in the merged image. (Scale bars, 20 μm.)

the Triton X-100–soluble and –insoluble fractions, presumably corresponding to the free and fibril-bound aggregates. Pα-syn* was also detected in a dimeric form at 25 kDa in the soluble and insoluble fractions of PFF-treated cells. In addition, the pα-syn* antibody also detected basal levels of full-length pα-syn (15-kDa band) present in the soluble fraction in both PBS- and PFF-treated cells. Both a C-terminal (encompassing amino acids 129–130) and an N-terminal (epitope ~5–25) α-syn antibody were able to detect pα-syn* (Fig. 3*I*, first three panels, red arrows). This shows that truncated pα-syn* resulted from a loss of ≤10 amino acids at the C terminus of pα-syn and ≤15 amino acids at the N terminus (Fig. 3*I*, scheme). Of note, a pα-synF antibody, while recognizing full-length pα-syn (Fig. 3*I*, fourth panel, green arrows), did not recognize the 12.5-kDa truncated pα-syn* species or the 25-kDa dimer thereof, emphasizing the differential immunoreactivity between pα-syn* and pα-synF (Fig. 3).

Together, these morphological and biochemical data show that pα-syn* results from partial proteolytic degradation of pα-synF. We hypothesize that C-terminal truncation of pα-synF, occurring at or close to amino acid 130, results in a conformational change of the epitope encompassing phosphorylated S129 along with conferring new immunoreactivity to pα-syn*.

Pα-Syn* Is a Result of Incomplete Autophagic Degradation of Pα-SynF. P62, an adaptor protein linking ubiquitinated protein aggregates to LC3 anchored in the membrane of the nascent autophagosome, labeled pα-synF (but not pα-syn*) with remarkable congruence (Fig. 3 *A*–*H*). This strongly suggested that pα-synF fibrils were undergoing autophagy and that pα-syn* may result from this proteolytic process. To confirm this hypothesis, we labeled PFF-treated cells with various markers recapitulating some major steps of autophagy. Ubiquitin, p62, and LC3 antibodies revealed fibrillar aggregates and largely excluded pα-syn* (Fig. 4 *A*–*C*). Pα-syn*, however, was found in LAMP1-positive lysosomes (Fig. 4*D*). These results confirmed that pα-synF underwent autophagy but that the autophagolysosomal digestion was incomplete, resulting in pα-syn*–bearing lysosomes. On the other hand, 20S proteasomal degradation seemed to be nonspecific. In cells containing abundant pα-synF, the 20S proteasome was found associated with pα-synF fibrils but not with pα-syn* aggregates (Fig. S4 *A* and *C*). In cells with low pα-synF load, the 20S proteasome also localized with pα-syn* (Fig. S4 *B* and *D*). In the situation of abundant pα-synF, the 20S proteasome subunit appeared up-regulated, as can be seen by the more abundant staining both in cytoplasm and nucleus compared with the PBS control or the low-fibril situation (Fig. S4). 20S proteasome up-regulation was observed starting at 8 days post PFF seeding in neurons with a high load of fibrils and seemed to be a reaction to the failure of the cells to contain large pα-synF fibrils. We performed a quantitative colocalization analysis. Fig. S4*E* shows the Manders' colocalization coefficients for pα-synF and pα-syn*, confirming our observations that the great majority of pα-synF was tagged by ubiquitin for degradation, subsequently engaging p62 and LC3. On the other hand, pα-syn* colocalized mostly

with LAMP1, and both pα-synF and pα-syn* colocalized with the 20S proteasome.

It appears that pα-synF fibril growth was highly dynamic and was accompanied by the simultaneous formation of pα-syn*, as we found pα-synF aggregates engulfed in LAMP1 vesicles (autophagolysosomes or lysosomes) at days 2–3, before fibrils were seen in the cells (Fig. 5 *A*–*C*, see small pα-syn* puncta in *B* and *C*) and when pα-synF forms short protofibrils (Fig. 5 *D*–*F*). Later on, when cells contained pα-synF fibrils, LAMP1 vesicles were found engulfing the core of the fibrils (Fig. 5*G*) or surrounding the fibrils (Fig. 5*H*) and always contained pα-syn* aggregates. The last step of pα-syn* formation was the exit from the lysosomes, depicted in Fig. 5 *I*–*K* (see arrows pointing to pα-syn* aggregates exiting disrupted lysosomes).

We used the fluorescent dye LysoTracker Red DND-99, which stains acidic organelles. In pα-syn*–laden lysosomes (Fig. 5*L*, arrows in the right enlarged square) LysoTracker DND-99 staining was absent, contrasting with the positive LysoTracker DND-99 signal in pα-syn*–negative, LAMP1-positive vesicles in the close vicinity. This observation suggests that lysosomes bearing pα-syn* inclusions lack the acidic internal environment, probably as a consequence of pα-syn* accumulation. Interestingly, some elongated vesicles showing weak LAMP1 staining but a good LysoTracker DND-99 signal contained pα-syn* inclusions organized in bead-like shapes, suggesting they were autophagolysosomes degrading a fibril (Fig. 5*L*, arrowheads in the left enlarged square pointing to pα-syn* aggregates in weakly LAMP1-positive vesicles).

Autophagy Modulation Affects the Formation of Pα-Syn*. As we found that pα-syn* results from autophagic degradation of pα-synF, we tested whether modulation of the autophagic flux would affect the rate of pα-syn* formation. Neurons were treated for 2.5 days (from day 3.5 postexposure to PFFs) with autophagy modulators and were examined at the end of the treatment. Treatment with rapamycin, an autophagy activator, resulted in the formation of larger (Fig. 6*B*) and more numerous (Fig. 6*E*) pα-syn* aggregates. Treatment with chloroquine, a compound disrupting lysosomal function, resulted in the net production of fewer pα-syn* aggregates (Fig. 6*E*); additionally, in a very few cells, we found a unique phenotype where cells exhibited numerous pα-syn* aggregates in the absence of pα-synF (Fig. 6*C*).

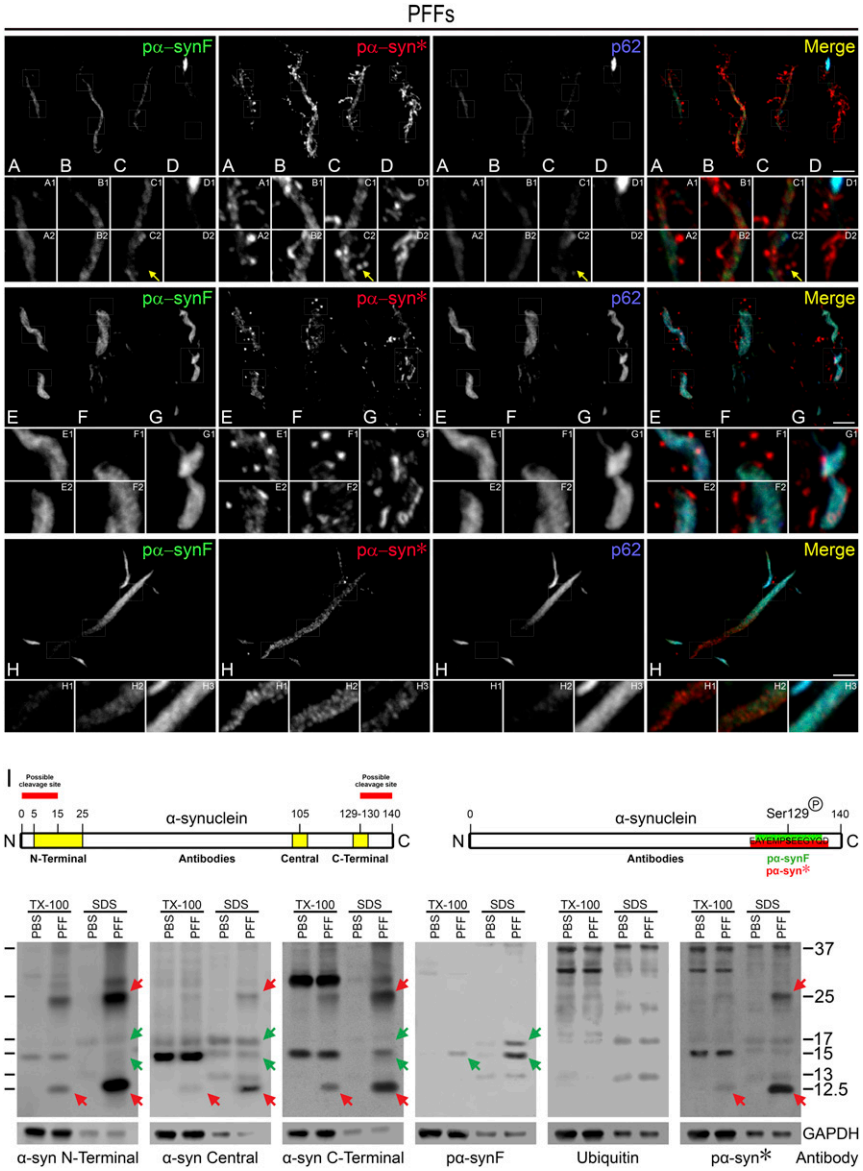

Fig. 3. Pα-syn* originates from partial degradation of pα-synF fibrils. (*A*–*D*) Thin pα-synF fibrils undergo conversion into pα-syn* in a patchy manner throughout the fibrillar core (*A1*, *B1*, *B2*) leading to the progressive disappearance of the pα-synF core and release of granular and serpentine pα-syn* structures. (*C2*) Pα-syn* beads (arrow). (*D*) Pα-synF core has entirely disappeared, leaving behind ribbons of pα-syn*. (*E*–*G*) Degradation of thick intertwined pα-synF fibrils: one strand is degraded first, leading to the release of granular pα-syn* surrounding the remaining strand. (*H*) A thick and straight pα-synF fibril is converted into pα-syn* starting from one end. *Insets H2* show the degradation front in the fibrillar core. Cells were labeled with pα-synF, pα-syn*, or p62 antibodies, color-coded as green, red, and blue, respectively, in the merged image. Note that p62 labeling is strictly restricted to pα-synF, showing that pα-synF undergoes autophagy while pα-syn* seems to be the product of the autophagic process. (*I*) The Western blots show detection of total α-syn using antibodies directed toward the N terminus, the central region, and the C terminus of α-syn recognizing the epitopes indicated in the scheme on the left, as well as pα-syn* using the pα-syn*–specific antibody (epitope indicated in the scheme on the right). Pα-syn*, labeled by red arrows, migrates at 12.5 kDa and is present specifically in PFF-treated neurons. A pα-syn* dimer is also detected at 25 kDa and is also specific for PFF-treated neurons. Pα-syn* is present in both the soluble (TX-100 extracted) and insoluble (SDS extracted) cellular fractions. A faint band corresponding to ubiquitinated pα-syn* is detectable at 13 kDa with the pα-syn* antibody, likely corresponding to immature pα-syn* attached to pα-synF, since mature pα-syn* aggregates are not ubiquitinated. Pα-syn* is also detectable using the N-terminal, central domain, and C-terminal total α-syn antibodies used for mapping purposes. Pα-synF is detected by a specific pα-synF antibody (epitope indicated in the scheme on the right) at 15 kDa corresponding to the full-length protein, as previously described, as well as at 17 kDa corresponding to the ubiquitinated form (green arrows). (Scale bars, 5 μm; *Insets* are a 3× magnification of the corresponding picture.)

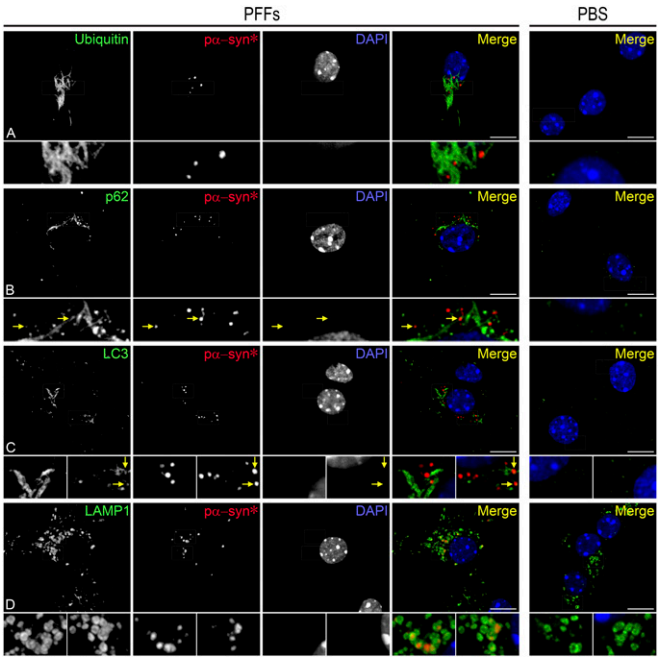

Fig. 4. Association of pα-synF and pα-syn* with markers of the autophagolysosomal pathway indicates that pα-syn* is the autophagic product of pα-synF. (*A*) Pα-synF fibrils are entirely covered with ubiquitin, tagging them for degradation (see also colocalization analysis in Fig. S4). (*B*) Pα-synF fibrils are tagged with the adaptor protein p62, targeting them for autophagic degradation. Arrows in *Insets* show nascent pα-syn* inclusions in direct contact with p62-tagged pα-synF fibrils. (*C*) LC3 covers pα-synF fibrils. Arrows in *Insets* show nascent pα-syn* inclusions in direct contact with LC3-tagged pα-synF fibrils. (*D*) Pα-syn* inclusions are contained in LAMP1-positive vesicles. Cells were labeled with ubiquitin, p62, LC3, LAMP1, and pα-syn* antibodies and DAPI, color-coded as green, red, and blue, respectively, in the merged images. (Scale bars, 10 μm; *Insets* are a 3× magnification of the corresponding picture.)

This phenotype contrasts with pα-syn* otherwise being always found in cells containing pα-synF. We hypothesize that chloroquine treatment, by disabling lysosomes, reduces the exit rate of pα-syn*, slows the phagocytic flux, and leads to a longer retention time of pα-synF in autophagosomes, resulting in more complete conversion of pα-synF into pα-syn*. This hypothesis also favors pα-syn* being generated in the autophagolysosomal pathway, consistent with our observation of pα-syn* inclusions in vesicles exhibiting features of autophagolysosomes (as described above; see Fig. 5*L*, left enlarged square). Finally, treatment with 3-Methyladenine (3-MA), a compound which impairs the formation of autophagosomes, led to a decrease in the number of pα-syn* aggregates generated (Fig. 6 *D* and *E*).

Overall, these data showed that the cellular autophagic activity level directly affects the rate of formation of pα-syn*.

After Lysosomal Release, pα-Syn* Targets Mitochondria. Before lysosomal release, nascent pα-syn* aggregates were found in the vicinity of mitochondrial networks but not colocalizing with them, and they sometimes harbored a serpentine morphology (Figs. 3 *A–D* and 7*A*). On the other hand, mature, granular pα-syn* aggregates were found abutting the end of mitochondrial tubules (Fig. 7*C*). We performed confocal and stimulated emission depletion (STED) nanoscopy (with spatial resolution <50 nm) to verify the direct association of pα-syn* aggregates with the outer mitochondrial membrane (labeled with Tom20). Pα-syn* was found colocalizing with Tom20 on mitochondrial tubules (Fig. 7 *D* and *E*). Fig. 7*F* shows smaller pα-syn* aggregates, allowing us to visualize the association with mitochondrial tubules and also with circular mitochondrial structures that might represent fissioned mitochondria (Fig. 7*F*, *Upper Inset*). Pα-syn* deposition was frequently associated with areas of mitochondrial fragmentation (Fig. 7*G*).

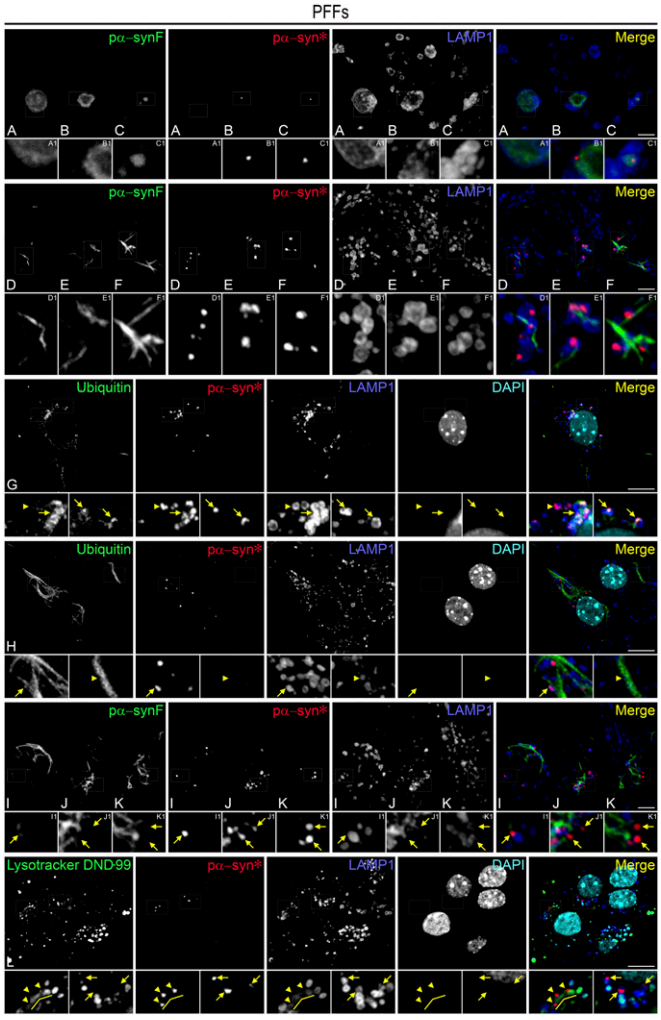

Fig. 5. Pα-syn* is found in autophagolysosomes and lysosomes. (*A–C*) Pα-synF aggregates are engulfed in LAMP1 vesicles (autophagolysosomes or lysosomes) at days 2–3, before fibrils are seen in the cells; small pα-syn* puncta are seen in *Insets B1* and *C1*. (*D–F*) Short protofibrils of pα-synF are being engulfed by LAMP1 vesicles. (*G*) Situation where a thin pα-synF fiber is being degraded within its core (as shown in Fig. 3 *A–D*), leading to an overlap of ubiquitin and LAMP1 staining (arrows). Pα-syn* detached from the core is not ubiquitin labeled (arrowhead) (*H*) A thick pα-synF fiber is releasing pα-syn*; there is no overlap between ubiquitin staining of the fibrillar core and pα-syn* labeling. The arrowhead shows an indent in the fibril coinciding with the presence of a lysosome. (*I–K*) Pα-syn* is seen exiting lysosomes (arrows in *I1*, *J1*, and *K1* point to pα-syn* aggregates exiting disrupted lysosomes). (*L*) Elongated vesicles positive for LysoTracker DND-99 and weakly labeled with LAMP1 and containing pα-syn* inclusions, organized in a chain-like shape, are likely to be autophagolysosomes degrading a fibril (arrowheads in the *Left Inset*). On the other hand, in LAMP1-positive pα-syn*–laden vesicles (arrows in the *Right Inset*) LysoTracker DND-99 staining is absent, indicating lack of the acidic internal environment of those organelles. In contrast, most LAMP1-positive, pα-syn*–negative vesicles in the close vicinity show a strong signal for LysoTracker DND-99. Cells were labeled with pα-synF and ubiquitin antibodies or LysoTracker DND-99, pα-syn*, and LAMP1 antibodies or DAPI, color-coded as green, red, blue, and turquoise, respectively, in the merged image. (Scale bars, 5 μm in *A–F* and *I–K*; 10 μm in *G*, *H*, and *L*; *Insets* are a 3× magnification of the corresponding picture.)

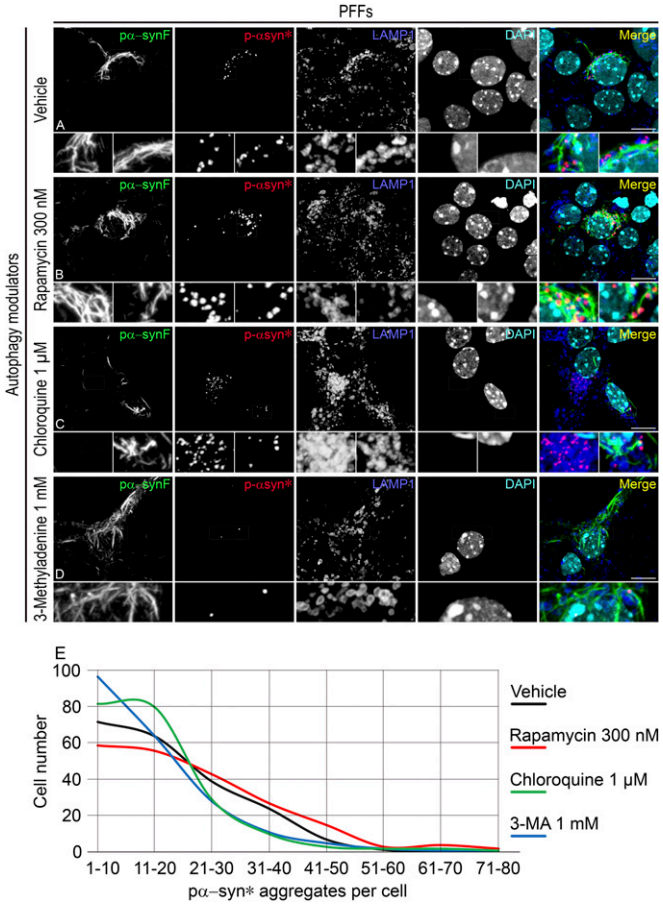

Fig. 6. Autophagy modulation alters the production of Pα-syn*. (*A–D*) Neurons were treated from day 3.5 post PFF exposure to day 6 post PFF exposure with the vehicle (*A*), rapamycin (*B*), chloroquine (*C*), or 3-MA (*D*) as indicated. Note the numerous and large pα-syn* aggregates in *B*. (*C*) The neuron on the right of the image (right enlarged area) shows few pα-syn* aggregates, while the neuron on the left of the image (left enlarged area) shows pα-syn* aggregates in the absence of pα-synF fibrils. (*D*) 3-MA treatment leads to fewer pα-syn* aggregates. (*E*) The number of pα-syn* aggregates per cell was counted in 200 cells of each culture in a blinded manner. The graph shows the number of cells bearing few (1–10) to numerous (71–80) aggregates under each culture condition. Cells were labeled with pα-synF, pα-syn*, and LAMP1 antibodies and DAPI, color-coded as green, red, blue, and turquoise, respectively, in the merged images of *A–D*. Pictures are Z-stacks of six confocal images to capture the total number of vesicles present in individual neurons. (Scale bars, 10 μm; *Insets* are a 3× magnification of the corresponding picture.)

Pα-Syn* Is Mitotoxic.

Pα-syn* induces depolarization of the inner mitochondrial membrane. MitoTracker Red CMXRos is a reagent that informs on the electrochemical gradient across the inner mitochondrial membrane and thereby scores the mitochondria's ability to perform oxidative phosphorylation and produce ATP (24). Mitochondrial labeling with MitoTracker Red CMXRos showed that pα-syn* was appended at the end of mitochondrial tubules that lacked membrane potential (Fig. S5 and Movie S1). To further demonstrate this point, we colabeled neurons for Tom20, a resident protein of the outer mitochondrial membrane that is part of the protein import machinery, and MitoTracker Red CMXRos. While the Tom20 antibody labeled the mitochondrial extremities to which pα-syn* was appended, MitoTracker Red CMXRos labeling was completely disrupted in such extremities (Fig. 8*B*; compare Fig. 8 *A* and *B* for colocalization of Tom20 and MitoTracker Red CMXRos in PBS-treated neurons). These data show that pα-syn* induces a loss of membrane potential in the portion of the mitochondria to which it is attached.

Pα-syn* induces cytochrome C release, mitochondrial fragmentation via pACC1, and mitophagy. At the mitochondrial membrane, pα-syn* usually localized to areas of increased cytochrome C staining (Fig. 9*A*, arrows). Cytochrome C accumulates in the mitochondrial intermembrane space as a result of a loss in mitochondrial potential and is then subsequently released after outer membrane permeabilization (25, 26). The observation of pα-syn* inclusions corresponding to zones of cytochrome C accumulation and release is consistent with the finding of a loss of mitochondrial potential in the areas of the mitochondrial tubules capped by pα-syn* aggregates (see above).

A striking observation was the extensive colocalization of pα-syn* with pACC1 (Fig. 9 *B*, *D*, and *E*). The filamentous pACC1 network was progressively lost in cells bearing pα-syn* aggregates starting at day 6, with recruitment of punctiform pACC1 to the mitochondria colocalizing with pα-syn* (Fig. 9*B*, arrows). ACC1 is involved in lipid metabolism via the production of malonyl CoA, a substrate for the synthesis of fatty acids that are essential for mitochondrial biogenesis (27–29). ACC1 is inactivated by phosphorylation (30). We propose that pα-syn* induces initial mitochondrial stress and a reduction in ATP production, resulting in high levels of AMP and activation of

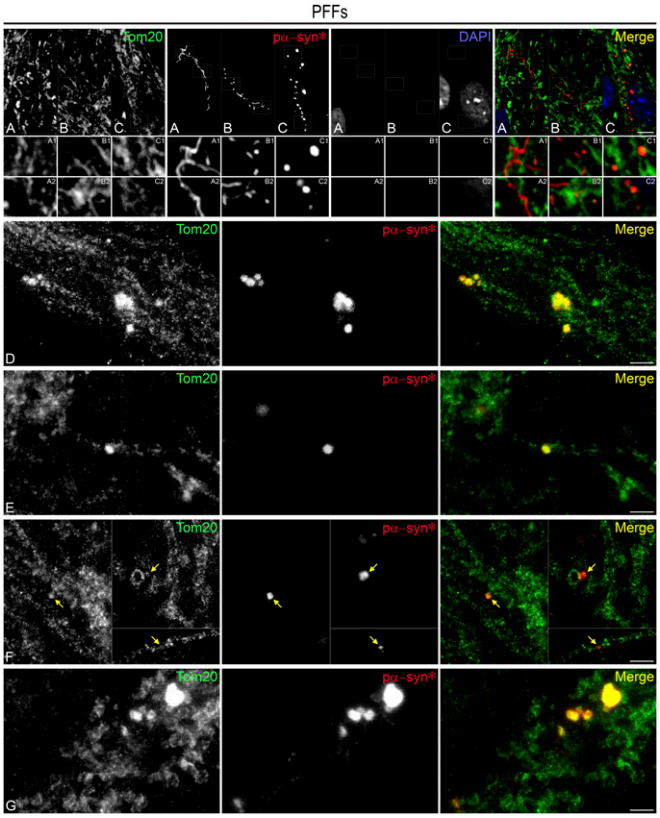

Fig. 7. Pα-syn* localizes to mitochondria and fragmented mitochondria. (*A*) Immature serpentine pα-syn* is present in the vicinity of but does not colocalize with mitochondria (*Insets A1* and *A2*). (*B* and *C*) Granular pα-syn* binds to mitochondrial tubules (*Insets C1* and *C2*). (*D–G*) STED nanoscopic imaging of pα-syn* aggregates attached to mitochondrial tubules (*D–F*). In *F*, arrows point to small pα-syn* aggregates associated with mitochondrial tubules or circular structures. (*G*) Large pα-syn* aggregates are associated with fragmented mitochondria. Cells were labeled with Tom20 antibody (mitochondrial outer membrane) and pα-syn*, color-coded as green and red, respectively, in the merged image. [Scale bars, 5 μm in *A–C*; 1 μm in (*D–G*); *Insets* are a 3× magnification of the corresponding picture.]

NEUROSCIENCE

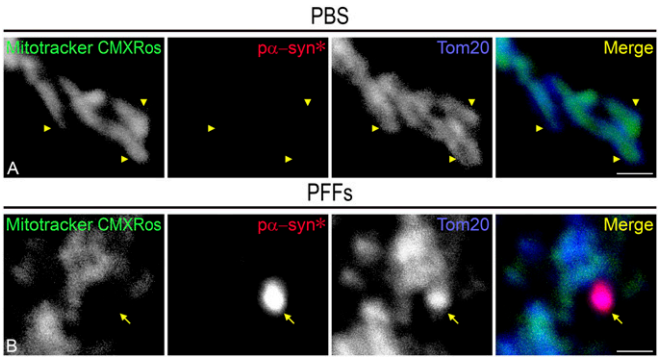

Fig. 8. Pα-syn* induces loss of mitochondrial membrane potential. (*A*) Tom20 and MitoTracker CMXRos labeling in PBS-treated cells is overlapping until the ends of the tubules (arrowheads). (*B*) Pα-syn* labeling colocalizes with Tom20 at the end of the mitochondrial tubule, but MitoTracker CMXRos is disrupted, showing a void area (arrow). Cells were labeled with MitoTracker CMXRos, pα-syn*, and Tom20 antibody, color-coded as green, red, and blue, respectively, in the merged images. (Scale bars, 1 μm.)

AMP-activated protein kinase (AMPK). Once activated, AMPK phosphorylates a number of targets, ACC1 being a major substrate. We further propose that the net increase of pACC1 at damaged mitochondria as a consequence of pα-syn* accumulation reproduces the effect of ACC1 knockdown, i.e., defective lipoylation and mitochondrial fragmentation (31). Thus, the extensive colocalization of pα-syn* with pACC1 strongly suggests that pα-syn* induces reduced energy levels and structural mitochondrial damage at least partly due to a loss of function of ACC1. Not surprisingly, pα-syn*/pACC1 staining colocalized with areas of cytochrome C release (Fig. 9*D*).

Pα-syn* colocalized with both Tom20 and BiP, a marker for the unfolded protein response (UPR) and a resident protein of MAMs, showing that pα-syn* localized to areas of mitochondria–MAMs contact (Fig. 9*C* and Fig. S6*A*). BiP and Tom20 colocalization was enhanced in PFF-seeded cultures compared with PBS controls. The quantitative colocalization analysis showed that about half of all cellular pα-syn* is associated with Tom20 and BiP at MAMs (Fig. 9*E*). Disturbances to MAM–mitochondrial contacts linked to mitochondrial stress signals have been found in several neurodegenerative diseases, including PD, AD, and amyotrophic lateral sclerosis (ALS), and constitute an area of increased scrutiny (32). MAMs were found to correspond to the sites of mitochondrial fission and autophagy induction (33, 34). Therefore, the fact that pα-syn* colocalizes with BiP at MAMs supports our data showing that pα-syn* induces structural and functional mitochondrial damage leading to mitochondrial fission and mitophagy. Mitophagy is a parkin-dependent process, since parkin tags areas of mitochondrial damage with ubiquitin to initiate mitophagic removal. We show in Fig. 10 *A* and *B* the presence of Tom20/pα-syn*–bearing mitophagic lysosomes colocalizing with parkin.

In contrast to the association of pα-syn* with the markers described above, we found no colocalization of pα-syn* with the endosome marker EEA1 (Fig. S6). We also found no direct association of pα-syn* with peroxisomes (using the marker catalase) (Fig. S6).

EM imaging of pα-syn*–bearing mitophagic vacuoles. Using EM and correlation light and EM (CLEM) analysis, we were able to superimpose pictures of immunofluorescence (IF) labeling of pα-syn* and cytochrome C (to localize areas of mitochondrial damage) with ultrastructural images. Examination of cells at a late stage (14 d after PFF exposure) revealed that virtually all pα-syn* aggregates were contained in mitophagic vacuoles (Fig. 10*C*; see the vacuoles labeled in red and containing medium-density deposits corresponding to proteinaceous aggregates). These mitophagic vacuoles were in direct contact with fragmented mitochondria (harboring green labeling for cytochrome C; see *Insets A* and *B* and enlarged images).

The Life Cycle of a Mitotoxic Pα-Syn Species Resulting from Failed Degradation of Pα-SynF Fibrils. Starting from our primary observation of pα-syn* as a unique conformational α-syn species, we performed a series of experiments to determine how pα-syn* was generated, to which cellular organelle it localized, and what were

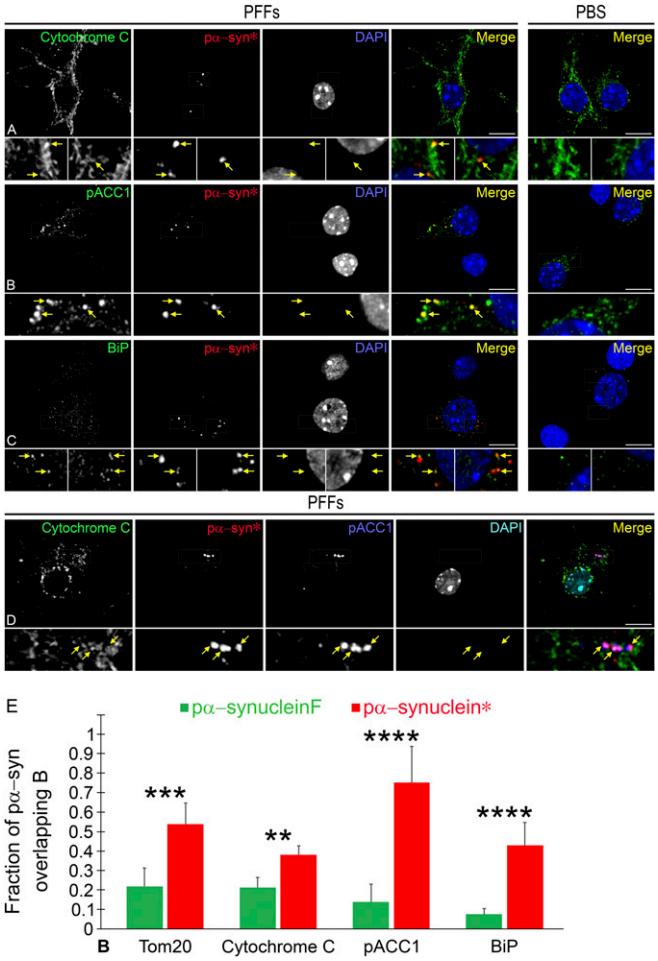

Fig. 9. Pα-syn* colocalizes with cytochrome C and pACC1 and is found in areas of mitochondrial–MAM tethering. (*A*) The points of contact of pα-syn* with the mitochondria correspond to zones of increased cytochrome C density (arrows in *Insets*). (*B*) A strong colocalization of pα-syn* is observed with pACC1 with pα-syn* inclusions completely overlapping with some pACC1 granules (arrows in *Insets*). (*C*) Pα-syn* also colocalizes with BiP, indicating that pα-syn* aggregates are located at the interface between the mitochondrial outer membrane and MAMs (arrows in *Insets*). (*D*) Recruitment of pACC1 to the sites of pα-syn* accumulation at damaged mitochondria. PACC1, pα-syn*, and cytochrome C labeling colocalize, with complete overlap of the pα-syn* and pACC1 labeling (arrows in *Insets*). In *A*–*C*, cells were labeled with cytochrome C, pACC1, BiP, and pα-syn*antibodies and DAPI, color-coded as green, red, and blue, respectively, in the merged images. In *D*, cells were labeled with cytochrome C, pα-syn*, pACC1 antibodies and DAPI, color-coded as green, red, blue, and turquoise, respectively, in the merged image. (Scale bars, 10 μm; *Insets* are a 3× magnification of the corresponding picture.) (*E*) Graph showing Manders' correlation coefficients of pα-syn* aggregates with markers of the outer mitochondrial membrane (Tom20), loss of integrity of mitochondrial membranes (cytochrome C), MAMs (BiP), and pACC1. Manders' coefficient of colocalization was calculated using IF intensities recorded in 15–20 neurons; ns, nonsignificant; $^{**}P < 0.01$; $^{***}P < 0.005$; $^{****}P < 0.001$.

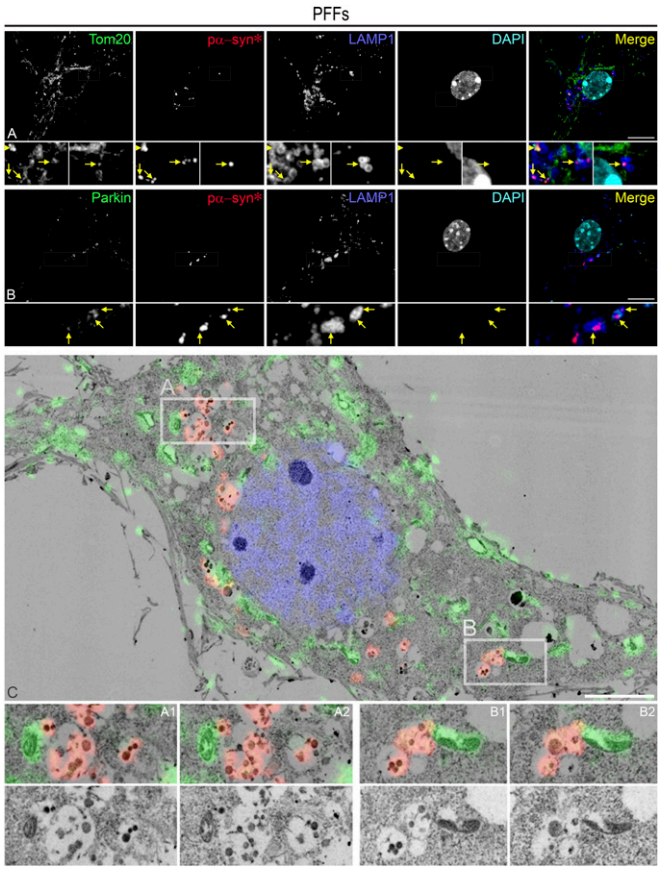

Fig. 10. Pα-syn* triggers mitophagy. (*A*) LAMP1-positive mitophagic vesicles in an area of mitochondrial network fragmentation contain pα-syn* and small Tom20 remnants (arrows in *Insets*). Arrowhead (*Left Insets*) shows a large pα-syn* aggregate colocalizing with Tom20. (*B*) Parkin, an E3-ubiquitin ligase orchestrating mitophagy at MAMs, colocalizes with pα-syn* containing LAMP1-positive mitophagic vesicles (arrows in *Insets*). Cells were labeled with Tom20, Parkin, pα–syn*, and LAMP1 antibodies and DAPI, color-coded as green, red, blue, and turquoise, respectively, in the merged images. (Scale bars, 10 μm.) (*C*) Electron micrograph of pα-syn*–bearing mitophagic vacuoles. Neurons at 14 d post PFF exposure were examined by IF for pα-syn* (red) and cytochrome C (green) and by EM for ultrastructural analysis, and images were superimposed. All pα-syn* aggregates were seen in mitophagic vacuoles also containing small electron-dense inclusions probably corresponding to mitochondrial debris. These mitophagic vacuoles were directly abutting cytochrome C-positive, fragmented mitochondria. Areas *A* and *B* were selected for enlarged images, and two adjacent EM sections (*A1*/*A2* and *B1*/*B2*) are shown with and without color overlay. (Scale bar, 5 μm; *Insets* of *A* and *B* are a 3× magnification of the corresponding picture; *Insets* of *C* are a 2x magnification of the corresponding picture.)

its biological effects. The life cycle of pα-syn* is depicted in Fig. 11. Our model is as follows: In PFF-seeded neurons, α-syn misfolds and forms primarily fibrillar pα-synF aggregates. Pα-synF activates autophagy. However, autophagolysosomal degradation is incomplete and/or abnormal, generating an N- and C-terminally trimmed pα-syn species, pα-syn*. The C-terminal truncation exposes a conformational epitope at the C terminus comprising pSer129, conferring pα-syn* unique immunoreactivity. Pα-syn* is generated in autophagolysosomes and impairs the lysosomes, from which it eventually exits. Pα-syn* then attaches to mitochondria where it induces functional damage (ACC1 inactivation, loss of mitochondrial potential associated with oxidative and energetic stress), structural damage (mitochondrial fragmentation), and cytochrome C release. Pα-syn* localizes to mitochondria–MAMs contacts (33) containing the misfolded protein response protein BiP (GRP78). MAMs are involved in parkin-dependent mitophagy induction (34) that results from pα-syn*–induced mitochondrial fission. The life cycle of pα-syn* ends with the mitophagic disposition of mitochondrial debris along with pα-syn*.

Discussion

PFFs are internalized into neurons in culture, leading to the recruitment of endogenous α-syn and the progressive accumulation of pα-syn inclusions reminiscent of LBs and LNs (herein called pα-synF) (14, 20). Pα-syn aggregates persist despite colocalizing with components of the autophagic and proteasomal protein degradation machineries; thus it has been suggested that the aggregates are refractory to clearance (22). Herein, we identified a unique conformation of pα-syn with immunoreactivity to a different pS129 α-syn antibody than that previously used to identify pα-synF. We named this pα-syn species pα-syn* due to its highly detrimental biological activity. Remarkably, pα-syn* is an N- and C-terminally trimmed pα-syn species generated by incomplete autophagolysosomal degradation of pα-synF. C-terminal truncations of α-syn by several proteases, such as calpain and cathepsin D, have been shown to promote fibrillization (35). Recently, an endolysosomal protease, asparagine endopeptidase, has been shown to cleave α-syn N-terminally in the brain of PD patients and to be involved in the pathogenesis of the disease (36).

In the light of our findings, we reinterpret the persistence and increase of pα-syn fibrils in neuronal cells as resulting from a highly dynamic system, where pα-syn fibrils are continuously degraded, as suggested by their tight association with markers of autophagic degradation, thereby generating pα-syn* that migrates away from the fibrils and mediates neurotoxicity. Growth of pα-synF fibrils is faster than fibril degradation, resulting in a

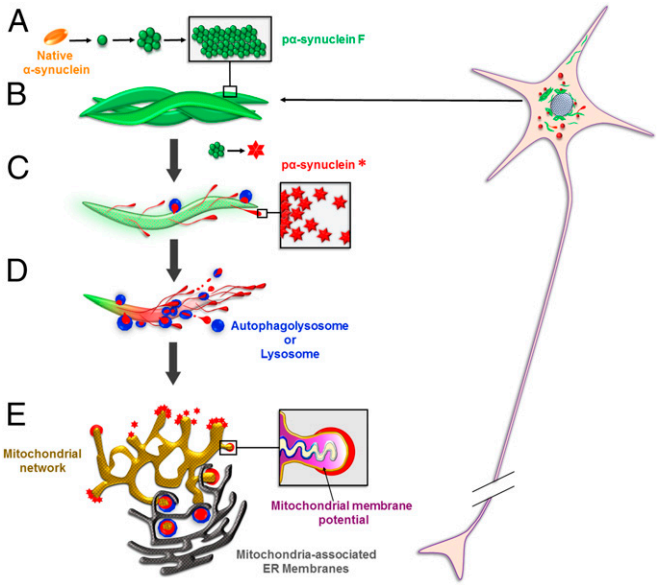

Fig. 11. Life cycle of pα-syn*. (*A*) In PFF-seeded neurons, endogenous α-syn misfolds and aggregates in the pα-synF conformation (depicted in green). (*B*) Pα-synF forms intertwined fibrils. (*C*) Pα-synF fibrils undergo autophagic degradation (Figs. 3 and 4). However, this process is incomplete, generating an N- and C-terminally trimmed pα-syn species with a different conformation, pα-syn* (depicted in red). (*D*) Pα-syn*-containing lysosomes are found in the pα-synF fibrillar core or on the fibril surface (Figs. 3 and 5). Autophagolysosomes/lysosomes are shown in blue. (*E*) Pα-syn* aggregates exit the lysosomes (Fig. 5) and localize to mitochondria (Fig. 7). Pα-syn* aggregates colocalize with MAMs (33), sites of Parkin-dependent mitochondrial fission and mitophagy (34). They induce mitochondrial membrane depolarization, cytochrome C release, oxidative and energetic stress, mitochondrial fragmentation, and mitophagy (Figs. 7–10).

net increase in cellular fibrillar content over time. This hypothesis is supported by our observation of pα-synF being engulfed by autophagolysosomal vesicles as early as day 3, when pα-synF is still in the protofibrillar stage (Fig. 5 *A–F*), with the appearance of "spots" of pα-syn*. Pα-synF then appears as increasingly long fibrils, sometimes entangled to form LB-like inclusions, but still being covered by autophagic markers and vesicles containing pα-syn*. Morphological variations in pα-synF fibrils result in a variety of appearances of the pα-synF degradation process (Fig. 3). Logically, then, analysis of Manders' colocalization coefficients showed that pα-synF colocalized preponderantly with ubiquitin, the autophagy adaptor protein p62, and the autophagosomal marker LC3, while pα-syn* colocalized mainly with LAMP1, labeling autophagolysosomes and lysosomes. Of note, the 20S proteasomal subunit decorated both pα-synF and pα-syn* (albeit pα-synF preferentially, since pα-syn* labeling was observed in low-fibril conditions) (Fig. S4), which is interpreted as nonspecific ubiquitin-independent degradation, as pα-syn* was rarely ubiquitinated. Indeed the 20S proteasomal subunit by itself has limited and nonspecific proteolytic activity in an ubiquitin-independent fashion (37).

PFF seeding of neurons has been shown to induce adverse effects such as defective vesicular transport (23), elevated dendritic mitochondrial oxidant stress (38), and synaptic dysfunction and neuronal death (20). It has been shown that pα-synF fibrils sequester endogenous α-syn, leading to a reduction of α-syn labeling at the dendritic spines, likely accounting, at least in part, for the synaptic dysfunction (20). On the other hand, there is overwhelming evidence for the involvement of mitochondrial pathology in PD (39, 40). However, the neurotoxic mechanisms underlying mitochondrial dysfunction and neuronal demise in PD are still largely unknown, and a direct relationship between the deposition of abnormal α-syn and mitochondrial damage has not been established. We propose that pα-syn* represents the missing link between LB deposition and mitochondrial toxicity.

Several facts support the role of pα-syn* as a major mitotoxic species. First, using confocal and STED microscopy, we observed that pα-syn* directly associates with mitochondrial tubules and with fragmented mitochondria. However, while pα-syn* colocalized extensively with the outer mitochondrial membrane protein Tom20, mitochondrial tubules capped by pα-syn* lacked MitoTracker Red CMXRos labeling, showing loss of inner membrane potential (Fig. 8*B*). These observations are in agreement with previous findings that cell treatment with aggregated α-syn leads to impairment of complex I of the electron transport chain and to reduced ATP and increased ROS production (41). A previous study also showed that a phosphomimetic mutant of α-syn, S129E, binds to Tom20 and inhibits mitochondrial protein import (42). Second, pα-syn* inclusions usually colocalized with areas of increased cytochrome C staining (Fig. 9 *A* and *D*). Cytochrome C accumulation occurs after mitochondrial inner membrane depolarization, and its release is thought to follow outer membrane permeabilization (25, 26). Third, pα-syn* remarkably colocalized with and sequestered pACC1 (Fig. 9 *B*, *D*, and *E*). ACC1 is phosphorylated upon AMPK activation due to increased AMP levels, ATP deprivation, and oxidative stress (27–29). ACC1 is listed in Mitocarta as a potential mitochondrial disease gene (43). The activity of mitochondrial ACC1 is necessary for fatty acid synthesis and mitochondrial biogenesis (31). Our data support the notion that pα-syn* induces the recruitment of phosphorylated and inactive ACC1 at the mitochondrial membranes, thereby leading to decreased lipoylation and mitochondrial fragmentation mimicking an AAC1-knockdown phenotype (31). Of note, AMPK has independently been found to mediate mitochondrial fission (44). Fourth, pα-syn* was found in the vicinity of or associated with BiP (Fig. 9*C*), a chaperone that is a master regulator of the UPR and a resident protein of the MAMs. MAMs are the sites of initiation of mitochondrial fission and Parkin-regulated mitophagy (33, 34). We observed pα-syn* inclusions in parkin-positive mitophagic vacuoles (Fig. 10*B*). EM imaging of late-stage PFF-exposed neurons showed that the majority of pα-syn* aggregates were found in mitophagic vacuoles abutting cytochrome C-positive, fragmented mitochondria (Fig. 10*C*). In summary, these findings position pα-syn* as a major mitotoxic species triggering ACC1 inactivation, structural and functional mitochondrial damage, and mitophagy.

The identification of pα-syn* raises the question as to whether this pα-syn species induces ACC1 phosphorylation solely via AMPK activation or in conjunction with other kinases. For example, JNK activation has been shown to be involved in mitochondrial dysfunction and dopaminergic cell loss in animal models of neurodegeneration (45, 46). The association of pα-syn* with BiP also entails UPR activation, which remains to be examined in detail. Other intriguing questions are whether pα-syn* is involved not only in neurotoxicity but also in intracellular templating of endogenous α-syn and whether pα-syn* is propagated intercellularly. We did not detect pα-syn* in the culture medium, but it might have been due to low levels. The role of exosomes as vectors of intercellular communication and material exchange is a fascinating area of biology, and exosomes contribute to the propagation of misfolded proteins and α-syn oligomers in particular (47). Extracellular pα-syn* also may simply result from neuronal death. Finally, the existence of an autoimmune response directed toward specific antigenic epitopes of pα-syn in 40% of PD patients has been recently described (48). Two major antigenic epitopes clusters were found, one being centered around Y39 (two epitopes) and the other around S129 (three epitopes). One of the three S129 epitopes comprises amino acids 116–130, corresponding to the C terminus of pα-syn*. Therefore, pα-syn* may be a player in driving the recently described autoimmune response. Indeed, our findings show that the exposure of phosphorylated S129 in pα-syn* changes the immunoreactivity of the trimmed protein, which loses reactivity toward the pα-synF antibody but becomes recognized by a different antibody.

We found that pharmacological activation of autophagy exacerbates the production of pα-syn*. In contrast, autophagy impediment reduces pα-syn* production (Fig. 6). These data show that any therapeutic approach aimed at accelerating the removal of fibrillary pα-syn aggregates/LBs with autophagy enhancers should be considered very carefully, as it might result in the production of more toxic and/or immunogenic pα-syn degradation products.

PD, like other PMNDs [AD, ALS, and Creutzfeldt–Jakob disease (CJD)] is primarily due to the misfolding and aggregation of a host protein causing neurotoxicity. For each of these diseases, the involvement of large protein aggregates (amyloid plaques in AD and CJD and LBs in PD) in neurotoxicity is a matter of intense scrutiny. The consensus emerged that oligomers, generated on or off the pathway to amyloid formation or resulting from fibril degradation, are primary players in protein-misfolding toxicity (49–52). The involvement of pα-syn in PD pathology was recognized exactly two decades ago (10), and numerous studies have examined the morphology and localization of α-syn aggregates (14, 53). Recently, the concept has emerged of the existence of different "strains" of α-syn aggregates by analogy to prions, which are aggregates of misfolded prion protein (54, 55). However, there was a need to identify toxic conformations of α-syn and define their relationship to Lewy pathology (56).

The present study uniquely describes pα-syn*, a small aggregate resulting from the failed degradation of pα-synF fibrils, made of a truncated and conformationally distinct form of pα-syn, and the direct link between pα-syn* and injured mitochondria as well as with molecular actors of metabolic stress signaling, mitochondrial fragmentation, and mitophagy. The relevance of

our findings is supported by the detection of pα-syn* not only in our cell culture model but also in the brains of mice injected with PFF and in PD patients' brains. We therefore propose that pα-syn* is a neurotoxic species central to the pathogenesis of PD and should be considered a therapeutic target.

Materials and Methods

All animal experiments were performed in accordance with protocols approved by the Scripps Florida Institutional Animal Care and Use Committee. *SI Materials and Methods* contains a list of reagents including pα-synF and pα-syn* antibodies and detailed descriptions of cultures of primary neurons, treatments, PFF production, autophagy modulation assays, mouse injections, protein extraction and Western blots, IF and brain immunochemistry, STED nanoscopy, EM and CLEM analysis, and statistical analyses.

ACKNOWLEDGMENTS. Funding was provided by National Institute of Neurological Disorders and Stroke Grant R01NS085223 (to C.I.L.), the Michael J. Fox Foundation (L.A.V.-D.), and the Saul and Theresa Esman Foundation (P.L.).

1. Lang AE, Lozano AM (1998) Parkinson's disease. *N Engl J Med* 339:1030–1053.
2. Olanow CW, Tatton WG (1999) Etiology and pathogenesis of Parkinson's disease. *Annu Rev Neurosci* 22:123–144.
3. Dawson TM (2005) Failures and successes of clinical trials for Parkinson disease treatments. *Retina* 25(8, Suppl):S75–S77.
4. Martin I, Dawson VL, Dawson TM (2011) Recent advances in the genetics of Parkinson's disease. *Annu Rev Genomics Hum Genet* 12:301–325.
5. Zhao F, et al. (2016) Mutations of glucocerebrosidase gene and susceptibility to Parkinson's disease: An updated meta-analysis in a European population. *Neuroscience* 320:239–246.
6. Athanassiadou A, et al. (1999) Genetic analysis of families with Parkinson disease that carry the Ala53Thr mutation in the gene encoding alpha-synuclein. *Am J Hum Genet* 65:555–558.
7. Krüger R, et al. (1998) Ala30Pro mutation in the gene encoding alpha-synuclein in Parkinson's disease. *Nat Genet* 18:106–108.
8. Zarranz JJ, et al. (2004) The new mutation, E46K, of alpha-synuclein causes Parkinson and Lewy body dementia. *Ann Neurol* 55:164–173.
9. Eriksen JL, Przedborski S, Petrucelli L (2005) Gene dosage and pathogenesis of Parkinson's disease. *Trends Mol Med* 11:91–96.
10. Spillantini MG, et al. (1997) Alpha-synuclein in Lewy bodies. *Nature* 388:839–840.
11. Spillantini MG, Crowther RA, Jakes R, Hasegawa M, Goedert M (1998) alpha-Synuclein in filamentous inclusions of Lewy bodies from Parkinson's disease and dementia with lewy bodies. *Proc Natl Acad Sci USA* 95:6469–6473.
12. Arima K, et al. (1998) NACP/alpha-synuclein immunoreactivity in fibrillary components of neuronal and oligodendroglial cytoplasmic inclusions in the pontine nuclei in multiple system atrophy. *Acta Neuropathol* 96:439–444.
13. Lippa CF, Schmidt ML, Lee VM, Trojanowski JQ (1999) Antibodies to alpha-synuclein detect Lewy bodies in many Down's syndrome brains with Alzheimer's disease. *Ann Neurol* 45:353–357.
14. Luk KC, et al. (2009) Exogenous alpha-synuclein fibrils seed the formation of Lewy body-like intracellular inclusions in cultured cells. *Proc Natl Acad Sci USA* 106: 20051–20056.
15. Luk KC, et al. (2012) Pathological α-synuclein transmission initiates Parkinson-like neurodegeneration in nontransgenic mice. *Science* 338:949–953.
16. Hansen C, et al. (2011) α-Synuclein propagates from mouse brain to grafted dopaminergic neurons and seeds aggregation in cultured human cells. *J Clin Invest* 121: 715–725.
17. Kordower JH, Chu Y, Hauser RA, Freeman TB, Olanow CW (2008) Lewy body-like pathology in long-term embryonic nigral transplants in Parkinson's disease. *Nat Med* 14:504–506.
18. Li JY, et al. (2008) Lewy bodies in grafted neurons in subjects with Parkinson's disease suggest host-to-graft disease propagation. *Nat Med* 14:501–503.
19. Volpicelli-Daley LA, Luk KC, Lee VM (2014) Addition of exogenous α-synuclein preformed fibrils to primary neuronal cultures to seed recruitment of endogenous α-synuclein to Lewy body and Lewy neurite-like aggregates. *Nat Protoc* 9:2135–2146.
20. Volpicelli-Daley LA, et al. (2011) Exogenous α-synuclein fibrils induce Lewy body pathology leading to synaptic dysfunction and neuron death. *Neuron* 72:57–71.
21. Oueslati A (2016) Implication of alpha-synuclein phosphorylation at S129 in synucleinopathies: What have we learned in the last decade? *J Parkinsons Dis* 6:39–51.
22. Tanik SA, Schultheiss CE, Volpicelli-Daley LA, Brunden KR, Lee VM (2013) Lewy body-like α-synuclein aggregates resist degradation and impair macroautophagy. *J Biol Chem* 288:15194–15210.
23. Volpicelli-Daley LA, et al. (2014) Formation of α-synuclein Lewy neurite-like aggregates in axons impedes the transport of distinct endosomes. *Mol Biol Cell* 25: 4010–4023.
24. Pendergrass W, Wolf N, Poot M (2004) Efficacy of mitotracker green and CMXrosamine to measure changes in mitochondrial membrane potentials in living cells and tissues. *Cytometry A* 61:162–169.
25. Bustamante J, Nutt L, Orrenius S, Gogvadze V (2005) Arsenic stimulates release of cytochrome c from isolated mitochondria via induction of mitochondrial permeability transition. *Toxicol Appl Pharmacol* 207(2 Suppl):110–116.
26. Martinou JC, Desagher S, Antonsson B (2000) Cytochrome c release from mitochondria: All or nothing. *Nat Cell Biol* 2:E41–E43.
27. Hardie DG, Scott JW, Pan DA, Hudson ER (2003) Management of cellular energy by the AMP-activated protein kinase system. *FEBS Lett* 546:113–120.
28. Douglas DN, et al. (2016) Oxidative stress attenuates lipid synthesis and increases mitochondrial fatty acid oxidation in hepatoma cells infected with hepatitis C virus. *J Biol Chem* 291:1974–1990.
29. Mackenzie RM, et al. (2013) Mitochondrial reactive oxygen species enhance AMP-activated protein kinase activation in the endothelium of patients with coronary artery disease and diabetes. *Clin Sci (Lond)* 124:403–411.
30. Kudo N, Barr AJ, Barr RL, Desai S, Lopaschuk GD (1995) High rates of fatty acid oxidation during reperfusion of ischemic hearts are associated with a decrease in malonyl-CoA levels due to an increase in 5′-AMP-activated protein kinase inhibition of acetyl-CoA carboxylase. *J Biol Chem* 270:17513–17520.
31. Monteuuis G, Suomi F, Kerätär JM, Masud AJ, Kastaniotis AJ (2017) A conserved mammalian mitochondrial isoform of acetyl-CoA carboxylase ACC1 provides the malonyl-CoA essential for mitochondrial biogenesis in tandem with ACSF3. *Biochem J* 474:3783–3797.
32. Paillusson S, et al. (2016) There's something wrong with my MAM; the ER-mitochondria axis and neurodegenerative diseases. *Trends Neurosci* 39:146–157.
33. van Vliet AR, Verfaillie T, Agostinis P (2014) New functions of mitochondria associated membranes in cellular signaling. *Biochim Biophys Acta* 1843:2253–2262.
34. Erpapazoglou Z, Corti O (2015) The endoplasmic reticulum/mitochondria interface: A subcellular platform for the orchestration of the functions of the PINK1-parkin pathway? *Biochem Soc Trans* 43:297–301.
35. Lashuel HA, Overk CR, Oueslati A, Masliah E (2013) The many faces of α-synuclein: From structure and toxicity to therapeutic target. *Nat Rev Neurosci* 14:38–48.
36. Zhang Z, et al. (2017) Asparagine endopeptidase cleaves α-synuclein and mediates pathologic activities in Parkinson's disease. *Nat Struct Mol Biol* 24:632–642.
37. Erales J, Coffino P (2014) Ubiquitin-independent proteasomal degradation. *Biochim Biophys Acta* 1843:216–221.
38. Dryanovski DI, et al. (2013) Calcium entry and α-synuclein inclusions elevate dendritic mitochondrial oxidant stress in dopaminergic neurons. *J Neurosci* 33:10154–10164.
39. Büeler H (2009) Impaired mitochondrial dynamics and function in the pathogenesis of Parkinson's disease. *Exp Neurol* 218:235–246.
40. Hsu LJ, et al. (2000) Alpha-synuclein promotes mitochondrial deficit and oxidative stress. *Am J Pathol* 157:401–410.
41. Reeve AK, et al. (2015) Aggregated α-synuclein and complex I deficiency: Exploration of their relationship in differentiated neurons. *Cell Death Dis* 6:e1820.
42. Di Maio R, et al. (2016) α-Synuclein binds to TOM20 and inhibits mitochondrial protein import in Parkinson's disease. *Sci Transl Med* 8:342ra78.
43. Calvo SE, Clauser KR, Mootha VK (2016) MitoCarta2.0: An updated inventory of mammalian mitochondrial proteins. *Nucleic Acids Res* 44:D1251–D1257.
44. Toyama EQ, et al. (2016) Metabolism. AMP-activated protein kinase mediates mitochondrial fission in response to energy stress. *Science* 351:275–281.
45. Hunot S, et al. (2004) JNK-mediated induction of cyclooxygenase 2 is required for neurodegeneration in a mouse model of Parkinson's disease. *Proc Natl Acad Sci USA* 101:665–670.
46. Chambers JW, Howard S, LoGrasso PV (2013) Blocking c-Jun N-terminal kinase (JNK) translocation to the mitochondria prevents 6-hydroxydopamine-induced toxicity in vitro and in vivo. *J Biol Chem* 288:1079–1087.
47. Danzer KM, et al. (2012) Exosomal cell-to-cell transmission of alpha synuclein oligomers. *Mol Neurodegener* 7:42.
48. Sulzer D, et al. (2017) T cells from patients with Parkinson's disease recognize alpha-synuclein peptides. *Nature* 546:656–661, and erratum (2017) 549:292.
49. Lesné S, et al. (2006) A specific amyloid-beta protein assembly in the brain impairs memory. *Nature* 440:352–357.
50. Winner B, et al. (2011) In vivo demonstration that alpha-synuclein oligomers are toxic. *Proc Natl Acad Sci USA* 108:4194–4199.
51. Simoneau S, et al. (2007) In vitro and in vivo neurotoxicity of prion protein oligomers. *PLoS Pathog* 3:e125.
52. Kayed R, et al. (2003) Common structure of soluble amyloid oligomers implies common mechanism of pathogenesis. *Science* 300:486–489.
53. Raiss CC, et al. (2016) Functionally different α-synuclein inclusions yield insight into Parkinson's disease pathology. *Sci Rep* 6:23116.
54. Guo JL, et al. (2013) Distinct α-synuclein strains differentially promote tau inclusions in neurons. *Cell* 154:103–117.
55. Prusiner SB, et al. (2015) Evidence for α-synuclein prions causing multiple system atrophy in humans with parkinsonism. *Proc Natl Acad Sci USA* 112:E5308–E5317.
56. Kalia LV, Kalia SK (2015) α-Synuclein and Lewy pathology in Parkinson's disease. *Curr Opin Neurol* 28:375–381.